

LOCAL TUNNELING CHARACTERISTICS NEAR A GRAIN BOUNDARY  
OF A  $D$ -WAVE SUPERCONDUCTOR AS PROBED BY A NORMAL-METAL  
OR A LOW- $T_C$ -SUPERCONDUCTOR STM TIP

A Thesis

by

HONGWEI ZHAO

Submitted to the Office of Graduate Studies of  
Texas A&M University  
in partial fulfillment of the requirements for the degree of  
MASTER OF SCIENCE

May 2005

Major Subject: Physics

LOCAL TUNNELING CHARACTERISTICS NEAR A GRAIN BOUNDARY  
OF A *D*-WAVE SUPERCONDUCTOR AS PROBED BY A NORMAL-METAL  
OR A LOW- $T_C$ -SUPERCONDUCTOR STM TIP

A Thesis

by

HONGWEI ZHAO

Submitted to Texas A&M University  
in partial fulfillment of the requirements  
for the degree of

MASTER OF SCIENCE

Approved as to style and content by:

---

Chia-Ren Hu  
(Chair of Committee)

---

Glenn Agnolet  
(Member)

---

Philip B. Yasskin  
(Member)

---

Edward Fry  
(Head of Department)

May 2005

Major Subject: Physics

## ABSTRACT

Local Tunneling Characteristics Near a Grain Boundary of a  $d$ -wave Superconductor  
as Probed by a Normal-metal or a Low- $T_c$ -superconductor STM Tip. (May 2005)

Hongwei Zhao, B.E., Jilin University, China;

M.S., Institute of Physics, Chinese Academy of Sciences, China

Chair of Advisory Committee: Dr. Chia-Ren Hu

We studied the local single-particle tunneling characteristics [as observed with scanning tunnel microscopy (STM)] for  $N - D$  and  $S - D$  tunneling, where  $N$  is a normal metal,  $S$  is a  $s$ -wave superconductor, and  $D$  is a  $d$ -wave superconductor with a  $\{100\}|\{110\}$  grain boundary. The tunneling Hamiltonian method was used. The self-consistent order parameter is first determined using the quasiclassical Green's-function method, and then the tunneling characteristics at various distances from the interface, reflectivity of the interface, and temperature are studied. For  $N - D$  tunneling, a zero-bias conductance peak (ZBCP) occurs near the interface with diminishing magnitude away from it. For  $S - D$  tunneling, the ZBCP splits to exhibit the gap of the  $s$ -wave low- $T_c$  superconducting tunneling tip and there is a range of negative conductance just outside the peaks when the tunneling point is near the grain boundary. The results are compared with those obtained by using a constant order parameter in each grain.

To Xuemei Wang

## ACKNOWLEDGMENTS

I would like to acknowledge my advisor Dr. Chia-Ren Hu for his patience and guidance during my graduate studies. I would like to thank him for his willingness to help me and never give up on me. I learned a lot from him. I would like to acknowledge Dr. Glenn Agnolet and Dr. Philip Yasskin for their help and kindness.

I would like to thank the secretaries at the physics department, especially Ms. Sandi Smith, for all help I received, especially her help with the signature collecting and the document submission when I was away from campus.

## TABLE OF CONTENTS

CHAPTER		Page
I	INTRODUCTION . . . . .	1
	A. Zero Energy Bound State (ZEBS) . . . . .	1
	B. Zero-bias Conductance Peak (ZBCP) . . . . .	2
II	SELF-CONSISTENT ORDER PARAMETER . . . . .	6
	A. Quasi-classical Green Function . . . . .	6
	B. Self-consistent Order Parameter . . . . .	11
III	TUNNELING CHARACTERISTICS . . . . .	15
	A. N-D Tunneling . . . . .	15
	1. Local Tunneling Current . . . . .	15
	2. Local Density of States . . . . .	24
	3. Discussions of Results . . . . .	27
	B. S-D Tunneling . . . . .	28
IV	CONCLUSIONS . . . . .	34
	REFERENCES . . . . .	36
	VITA . . . . .	40

## LIST OF FIGURES

FIGURE		Page
1	Schematic drawing showing a scanning tunneling microscopy/ spectroscopy (STM/S) tip scanning the vicinity of a $\{100\} \{110\}$ grain boundary of a $d$ -wave superconductor. The tunneling direction is along the $c$ axis in this figure, but it doesn't have to be so. . . . .	7
2	Plot of the normalized self-consistent superconducting order parameter as a function of $x$ at four values of the interface reflectivity $r$ and two values of the temperature $T$ : Upper panel: $T = 0.1T_{cd}$ ; Lower panel: $T = 0.025T_{cd}$ . . . . .	13
3	Normalized local tunneling conductance $G$ between a normal-metal STM/S tip and a $d$ -wave superconductor with a $\{100\} \{110\}$ grain boundary, as a function of the applied voltage $V$ . Part (a) is for four values of $x$ (in units of $\xi_0$ ) on the $\{100\}$ side (i.e., the negative $x$ side), and part (b) is for four values of $x$ on the $\{110\}$ side (i.e., the positive $x$ side). The grain-boundary reflectivity parameter is assumed to be $r = 0$ here, and the temperature is assumed to be $T = 0.025T_{cd}$ . Solid lines are obtained using the self-consistent order parameter, and the dashed lines are obtained by assuming a constant order parameter on each side. A width parameter for the quasi-particle eigenstates has been taken to be $\delta = 0.05T_{cd}$ . With 100% transmission at the grain boundary assumed here, the local conductance shows no discontinuity at $x = 0$ . . . . .	17
4	Same as Fig. 3 except that $r = 0.3$ in this figure. The local conductance is now discontinuous at $x = 0$ . That is, the plots at $x = \pm 0$ are now different. . . . .	18
5	Same as Fig. 4 (or 3) except that $r = 0.7$ in this figure. . . . .	19

## FIGURE

## Page

6	Same as Fig. 4 (or 3) except that $r = 1.0$ in this figure. This case corresponds to the sample split into a semi-infinite sample with a $\{100\}$ surface situated at $x < 0$ , and a semi-infinite sample with a $\{110\}$ surface situated at $x > 0$ . The ZBCP then shows up on the $x > 0$ side only, near $x = 0$ , where midgap surface states exist. . . . .	20
7	Same as Fig. 5 except that the temperature $T = 0.1T_{cd}$ . This figure is to illustrate the temperature effect. . . . .	21
8	The height of the ZBCP is plotted as a function of the distance $x$ away from the interface for different values of $r$ . $T = 0.025T_{cd}$ is assumed. . . . .	23
9	Plot of $n(x, \theta, E)$ at $E = 0$ as a function of $x$ for four values of $r$ at $\theta = (3/16)\pi$ . Part (a) is obtained using the self-consistent order parameter, and part (b) is obtained by assuming a constant order parameter in each grain. . . . .	25
10	Same as Fig. 9 except that $\theta = (3/8)\pi$ . . . . .	26
11	Same as Fig. 5 except that the STM/S tip is now assumed to be made of a low- $T_c$ $s$ -wave superconductor with $T_{cs} = 0.1T_{cd}$ . The temperature $T = 0.025T_{cd}$ is $\ll T_{cs}$ so we have approximated $\Delta_s(T)$ by $\Delta_s(0)$ . . . . .	30
12	The $I(V)$ characteristics corresponding to the normalized conductance plotted in Fig. 11. The current peak in this plot gives rise to the negative conductance in Fig. 11. . . . .	31



## FIGURE

Page

- 13      Plotted is the normalized local tunneling conductance  $G$  between a low-temperature  $s$ -wave superconductor STM/S tip and a  $d$ -wave superconductor containing a  $\{100\}|\{110\}$  grain boundary as a function of the applied voltage  $V$  at six values of  $x$  (in units of  $\xi_0$ ), showing the effect of the temperature  $T$  as it is raised from much below  $T_{cs}$  ( $= 0.1T_{cd}$ ) toward  $T_{cs}$ . The gap of the low-temperature,  $s$ -wave superconductor is seen to gradually close up in the (split) zero-bias conductance peak. Part (a) is for three values of  $x$  on the  $\{100\}$  side (i.e., the  $x < 0$  side), and part (b) is for three values of  $x$  on the  $\{110\}$  side (i.e., the  $x > 0$  side). The negative conductance just outside the split ZBCP is seen to occur only at temperatures  $T \ll T_{cs}$  only. . . . . 33

## CHAPTER I

### INTRODUCTION\*

There has been a large number of experiments studying the symmetry of the order parameter in high- $T_c$  superconductors, because this information is crucial for understanding the mechanism of this class of superconductors. A large number of models and calculations have also been presented, and most of them suggest that the conventional  $s$ -wave pairing is unfavorable for high  $T_c$  superconductivity. They strongly suggest the possibility of  $d_{x^2-y^2}$ -wave pairing. Several phase-sensitive experiments [1, 2, 3, 4] have observed the sign change of the order parameter on the essentially cylindrical Fermi surface, which supports the conclusion that the order parameter of high- $T_c$  superconductors has predominantly a  $d_{x^2-y^2}$ -wave symmetry.

#### A. Zero Energy Bound State (ZEBS)

For the  $d_{x^2-y^2}$ -symmetry model, the existence of zero-energy (quasi-particle) bound states (ZEBS's, also called the midgap states) on the surface has been predicted. [5] The reason for their existence is that the incident and reflected quasiparticles see different sign of the order parameter. This sign change of the order parameter results in a new type of Andreev reflection, and the repeated Andreev reflections at the surface form the ZEBS. The number of the ZEBS's depends on the orientation of the surface

---

This thesis follows the style of Physical Review B.

\*Modified with permission from “Local tunneling characteristics near a grain boundary of a  $d$ -wave superconductor as probed by a normal-metal or a low- $T_c$ -superconductor STM tip” as follows: Hongwei Zhao and Chia-Ren Hu, *The Physical Review B*, 62, 1308-1318, 2000. Copyright (2000) by the American Physical Society.

with respect to the crystal axis. It has a maximum for a  $\{110\}$  surface and a minimum (*i.e.*, zero) for a  $\{100\}$  surface. [6] (According to Refs. [7, 8], the ZEBS's can also exist on a microscopically rough  $\{100\}$  surface.) The discussion can be directly generalized to an interface (*i.e.*, a grain boundary) of a d-wave superconductor, but the condition for the existence of the ZEBS's is more restrictive. [9, 10] Namely, both the reflected and the transmitted quasiparticles have to see different sign of the order parameter from that seen by the incident quasi-particle.

There are many novel properties related to the midgap states [11], such as the zero bias conductance peak (ZBCP) in single particle tunneling when performed on high- $T_c$  superconductors, a low temperature anomaly in the magnetic penetration depth, a non-Frauenhofer magnetic field dependence of the Josephson critical current of a  $\{110\}|\{100\}$  junction, midgap states induced paramagnetic Meissner effect, giant magnetic moment and resonant *ac* Josephson effect, etc.; some of them have been observed in experiments. The details about the predicted and observed consequences of the midgap states can be found in Ref. [11].

## B. Zero-bias Conductance Peak (ZBCP)

Zero-bias conductance peak (ZBCP) in quasi-particle tunneling is one of the distinct features related to the high  $T_c$  superconductors, which has been observed in many experiments. [12, 13, 14, 15, 16, 17, 18, 19, 20, 21, 22, 23, 24, 25, 26, 27, 28, 29, 30] ZEBS explains the origin of the ZBCP [5, 31]: The peak in the quasiparticle density of states at the Fermi surface due to the ZEBS leads to the ZBCP in the quasiparticle tunneling spectra of normal metal/*d*-wave superconductor junctions. Fogelstrom *et al.* [7] then concluded that a pure d-wave order parameter can induce an s-wave

sub-dominant component near the surface because of the strong pair-breaking property of a surface to d-wave superconductivity. The two order parameter components have a relative phase difference of  $\pi/2$ , and the resultant  $d + is$  order parameter at sufficiently low temperatures near the surface gives rise to a broken-time-reversal-symmetry (BTRS) state, which causes the energy of a ZEBS to shift away from zero by an amount which is dependent on its momentum along the surface in the  $ab$  plane. This energy shift gives rise to a splitting of the ZBCP at zero magnetic field and further nonlinear splitting with increasing external field, which appears to have been observed. [23, 24, 25] Asano *et al* [32] discussed the splitting of the ZBCP due to the impurity scattering near the interface of normal metal and the  $d$ -wave superconductor. This splitting is a consequence of the interplay between two effects of the impurity scattering: (i) drastically suppressing the conductance around the zero bias voltage and (ii) making the conductance peak wider. [32]

Originally, the observed ZBCP was analyzed in terms of the spin-flip and Kondo scatterings from the magnetic impurities which were presumed to exist at or near the interface. But this interpretation has been challenged by the experimentally observed [18, 21] *nonlinear* dependence of the ZBCP splitting on the applied magnetic field, and also by the absence of a ZBCP for the electron-doped, presumably s-wave cuprate superconductors [18, 19, 20, 33]. Furthermore, that the ZBCP is continuously observed with scanning tunneling microscopy/spectroscopy (STM/S) for a long distance (160nm) on a  $\{110\}$  surface, with nearly a constant height, is strongly against the impurities scenario; [17] and that a ZBCP is consistently observed on a  $\{110\}$  surface, and consistently not observed on a  $\{100\}$  surface, is also strongly in favor of the midgap-states scenario. [27] Therefore, the observation of the ZBCP in high- $T_c$  superconductors can nowadays be regarded as a strong evidence for the  $d_{x^2-y^2}$ -wave

order-parameter symmetry in this class of SC's (i.e., the hole-doped cuprates, with the electron-doped cuprates not as clear). The ZBCP was also observed on the  $\{100\}$  surface [26] which is attributed to the roughness of the surface. [7, 8] For tunneling between a low  $T_c$  superconductor and a high- $T_c$  superconductor, a splitting of the ZBCP at zero magnetic field was observed, [12] and the conductance at zero bias decreases with decreasing temperature. Because this splitting only occurs when the temperature is below the  $T_c$  of the low  $T_c$  superconductor, it can not be attributed to the BTRS states. It is explained as due to the convolution between the quasi-particle density of states of the low  $T_c$  superconductor and that of the high- $T_c$  superconductor. [9]

The ZEBS is a quasi-particle state localized near a surface or an interface. We expect that this localization can be observed in an STM/S type of localized quasi-particle tunneling: The ZBCP is expected to have a maximum height when the tunneling occurs at the surface or interface and to decrease in height when the tunneling point moves away from the surface or interface. [34] In this paper, we study the local characteristics for tunneling between an STM/S tip and a d-wave superconductor with a grain boundary (as shown in Fig. 1). [35] We assume that the left grain is  $\{100\}$  oriented and the right grain is  $\{110\}$  oriented. The angular dependence of the order parameter is  $\Delta_L(\theta) = \cos(2\theta)$  and  $\Delta_R(\theta) = \sin(2\theta)$ , for the left and right grains, respectively, where  $\theta$  is the angle between a two-dimensional relative momentum vector of the pairs in the  $ab$  plane and the surface normal. When the tip scans in the  $xy$  plane, the tunneling can occur at different points relative to the grain boundary. We expect the order parameter changes dramatically near the interface, especially on the  $\{110\}$  side because of the formation of the ZEBS's. Therefore we need self-consistently calculate the order parameter to include spatial dependence. The value of the order parameter near the interface also depends on the reflectivity of the interface

because there exists the proximity effect. We will use the quasi-classical Green function method to calculate the self-consistent order parameter, and then the tunneling conductance for different interface reflectivities. We will also compare the results at different temperatures.

A high- $T_c$  superconductor can, to a good approximation, be considered as a two-dimensional (2-D) system. If we assume translational invariance along the grain boundary, we expect the spatial dependence of the tunneling characteristics to depend on one coordinate only, *viz.*, the coordinate  $x$  measured perpendicular to the grain boundary. We will study the local tunneling characteristics when the tip is either a normal metal (N) or a low  $T_c$  superconductor (S).

This thesis is organized as follows: Chapter II briefly introduces the method of quasi-classical Green functions for the calculation of the self-consistent order parameter. In chapter III, we present the tunneling conductance for the tip being a normal metal and a low  $T_c$  superconductor. Finally, we make conclusions in chapter IV.

## CHAPTER II

### SELF-CONSISTENT ORDER PARAMETER\*

The model we considered is shown in Fig. 1. The grain boundary (interface) is located at  $x = 0$ . We assume that the left hand side of the interface is a  $\{100\}$  grain and the right hand side is a  $\{110\}$  grain. An STM/S type tunneling can occur at different distances (*i.e.*,  $x$ 's) away from the interface.

#### A. Quasi-classical Green Function

In order to calculate the tunneling conductance accurately at different tunneling points, first we need to calculate the spatially varying self-consistent order parameter. We use the quasi-classical Green function method [36, 37, 38] to calculate this quantity. The order parameter can be expressed as:

$$\begin{aligned}\Delta(\mathbf{r}, \mathbf{r}') &= V(\mathbf{r}, \mathbf{r}') < \Psi_{\uparrow}(\mathbf{r}) \Psi_{\downarrow}(\mathbf{r}') > \\ &= TV(\mathbf{r}, \mathbf{r}') \sum_n \sum_l \frac{u_l(\mathbf{r}) v_l^*(\mathbf{r}')}{i\varepsilon_n - E_l},\end{aligned}\tag{2.1}$$

where  $V(\mathbf{r}; \mathbf{r}')$  is the pair interaction;  $T$  is the absolute temperature;  $\varepsilon_n \equiv (2n+1)\pi T$  is the Matsubara frequency;  $u_l$  and  $v_l$  satisfy the Bogoliubov de Gennes equations with eigenenergy  $E_l$ :

$$E_l u_l(\mathbf{x}_1) = \hat{h}_0 u_l(\mathbf{x}_1) + \int \Delta(\mathbf{s}, \mathbf{r}) v_l(\mathbf{x}_2) d\mathbf{x}_2,\tag{2.2}$$

$$E_l v_l(\mathbf{x}_1) = -\hat{h}_0 v_l(\mathbf{x}_1) + \int \Delta(\mathbf{s}, \mathbf{r}) u_l(\mathbf{x}_2) d\mathbf{x}_2.\tag{2.3}$$

---

\*Modified with permission from “Local tunneling characteristics near a grain boundary of a  $d$ -wave superconductor as probed by a normal-metal or a low- $T_c$ -superconductor STM tip” as follows: Hongwei Zhao and Chia-Ren Hu, *The Physical Review B*, 62, 1308-1318, 2000. Copyright (2000) by the American Physical Society.

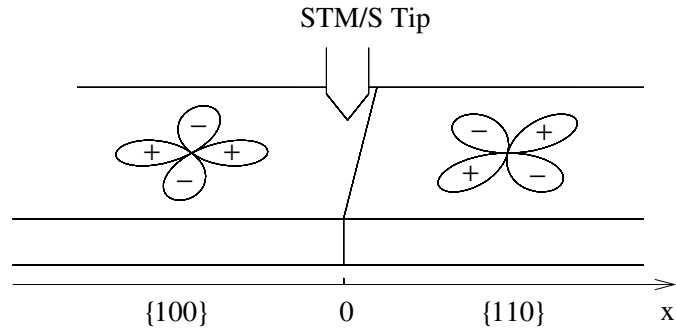


Fig. 1. Schematic drawing showing a scanning tunneling microscopy/ spectroscopy (STM/S) tip scanning the vicinity of a  $\{100\}|\{110\}$  grain boundary of a  $d$ -wave superconductor. The tunneling direction is along the  $c$  axis in this figure, but it doesn't have to be so.



Where  $\mathbf{s} \equiv (\mathbf{x}_1 - \mathbf{x}_2)$ ,  $\mathbf{r} \equiv (\mathbf{x}_1 + \mathbf{x}_2)/2$ , and  $\hat{h}_0 \equiv -\hbar^2 \nabla_{\mathbf{x}_1}^2 / 2m - \mu$  in the absence of a magnetic field and any other fields, with  $\mu$  the chemical potential. In the WKBJ approximation, the wave function has the form:

$$\begin{pmatrix} u(\mathbf{x}) \\ v(\mathbf{x}) \end{pmatrix} = e^{i\mathbf{k}_F \cdot \mathbf{x}} \begin{pmatrix} \bar{u}(x) \\ \bar{v}(x) \end{pmatrix}, \quad (2.4)$$

where  $k_F$  is the Fermi momentum.  $\bar{u}(x)$  and  $\bar{v}(x)$  vary on a scale of the coherent length  $\xi_0$ , which is much larger than the Fermi wave length  $k_F^{-1}$ . According to the 2-D property of high  $T_c$  superconductors, and if we assume the translational invariance of the interface,  $\bar{u}$ ,  $\bar{v}$ , and  $\Delta$  depend on  $x$  only. Substitution of Eq. (2.4) into Eqs. (2.2),(2.3), and neglecting the second-order differential terms lead to the Andreev equations:

$$E \bar{u}(x) = -iv_{Fx} \frac{d}{dx} \bar{u}(x) + \Delta(\hat{\mathbf{k}}, x) \bar{v}(x), \quad (2.5)$$

$$E \bar{v}(x) = iv_{Fx} \frac{d}{dx} \bar{v}(x) + \Delta(\hat{\mathbf{k}}, x) \bar{u}(x), \quad (2.6)$$

where  $\Delta(\mathbf{k}, x)$  is the order parameter after a Fourier transformation with respect to the relative coordinate  $\mathbf{s}$ . *I.e.*,  $\mathbf{k}$  is the relative wave-vector.  $v_{Fx}$  is the  $x$ -component of the Fermi velocity along  $\mathbf{k}$ . For the order parameter in Eqs. (2.5) and (2.6), only the direction of the wave-vector,  $\hat{\mathbf{k}} = \mathbf{k}/|\mathbf{k}|$ , is retained as a variable, because the momentum can be fixed on the Fermi surface in the weak-coupling treatment. To simplify the notation, we have suppressed the  $\hat{\mathbf{k}}$ -dependence in  $\bar{u}$  and  $\bar{v}$ .

If we assume partial specular reflection (with probability  $r$ ) and partial forward transmission (with probability  $t = 1 - r$ ) at the interface, the  $y$ -component of the momentum of a quasi-particle will be still  $k_y$  after a reflection, but the  $x$  component of the momentum will change sign. Therefore, the wave function should be a linear

combination of two terms on each side of the interface:

$$\begin{pmatrix} u_l(x, y) \\ v_l(x, y) \end{pmatrix} = e^{ik_y y} \sum_{\alpha=+,-} \phi_{l\alpha}(x, \theta_\alpha) e^{\alpha i k_x x}, \quad (2.7)$$

where  $\theta_\alpha$  measures the direction of the momentum  $(\alpha k_x, k_y)$  with respect to the  $x$ -axis.  $+$  and  $-$  mean right and left moving, respectively.  $\theta_+ = \theta$  with  $-\pi/2 < \theta < \pi/2$  gives the direction of a right-moving electron, and  $\theta_- = \pi - \theta$  gives that of a left-moving electron.  $k_x = k_F \cos \theta > 0$  and  $k_y = k_F \sin \theta$  are the  $x$ - and  $y$ -components of a right-going momentum vector, respectively, and

$$\phi_{l\alpha} = \begin{pmatrix} \bar{u}_{l\alpha} \\ \bar{v}_{l\alpha} \end{pmatrix}. \quad (2.8)$$

After applying a Fourier transformation to Eq. (2.1), the order parameter can be expressed as [36, 37, 39]

$$\Delta(\theta, x) = \frac{Tm}{4\pi} \sum_{n, \alpha=\pm} \int_{-\frac{\pi}{2}}^{\frac{\pi}{2}} d\theta' [\hat{g}_{\alpha\alpha}(x, \theta'_\alpha, \varepsilon_n) V(\theta, \theta'_\alpha)]_{12}, \quad (2.9)$$

where each  $\hat{g}_{\alpha\beta}$  is a  $2 \times 2$  matrix in the particle-hole space. It is known as the quasi-classical Green function. The subscript 12 means the element 12 of this matrix. The following defining equation:

$$\hat{g}_{\alpha\beta}(x) \pm i(\gamma_3)_{\alpha\beta} \hat{1} = -2v_{Fx} \hat{\rho}_3 \hat{G}_{\alpha\beta}(x \pm 0, x), \quad (2.10)$$

relates  $\hat{g}_{\alpha\beta}$  to  $\hat{G}_{\alpha\beta}(x, x')$ , which is the Gor'kov Green's function, a  $2 \times 2$  matrix in the particle-hole space, further converted to a  $2 \times 2$  matrix in the “directional space”, with indices  $\alpha\beta$ , so that the rapidly oscillating factors can be removed: [36]

$$\hat{G}_{\alpha\beta}(x, x') = \sum_l \frac{\phi_{l\alpha}(x) \phi_{l\beta}^+(x')}{i\varepsilon_n - E_l}, \quad (2.11)$$

where the  $l$ -sum is now confined to the sum over the quantum number in association with the  $x$ -motion only, since the sum over  $k_y$  has been turned into an integral over  $\theta'$  in Eq. (2.9). (The  $l$ -sum in Eq. (2.1) includes the sum over both quantum numbers.) In Eq. (2.10),  $\gamma_3$  is the third Pauli matrix in the directional (i.e.,  $+$   $-$ ) space;  $\rho_3$  is the third Pauli matrix in the particle-hole space; and  $\hat{1}$  is the unit matrix in the particle-hole space. To simplify the notation, we have left out the variables  $\theta$  and  $\varepsilon_n$  in  $\hat{g}_{\alpha\beta}$  and  $\hat{G}_{\alpha\beta}$  in Eqs. (2.10) and (2.11). In Eq. (2.9), We have omitted the  $\hat{g}_{+-}$  and  $\hat{g}_{-+}$  terms because their contributions are rapidly oscillating in the scale of Fermi wavelength. The quasi-classical Green function  $\hat{g}_{\alpha\beta}$  satisfies the following differential equation: [37]

$$iv_{F_x}\partial_x\hat{g}_{\alpha\beta} = -\alpha(i\varepsilon_n\hat{1} - \hat{\Delta}_\alpha)\hat{\rho}_3\hat{g}_{\alpha\beta} + \hat{g}_{\alpha\beta}\beta(i\varepsilon_n\hat{1} - \hat{\Delta}_\beta)\hat{\rho}_3, \quad (2.12)$$

where

$$\hat{\Delta}_\alpha = \begin{pmatrix} 0 & \Delta(\theta_\alpha, x) \\ \Delta^*(\theta_\alpha, x) & 0 \end{pmatrix}. \quad (2.13)$$

In order to solve the differential equation (2.12), we need the boundary conditions of the quasi-classical Green function  $\hat{g}_{\alpha\beta}$  at the interface and the two end points:  $x = -L_L$  and  $L_R$ . (Eventually, we will let  $L_L$  and  $L_R$  go to infinity.) The boundary condition at the interface is [36]:

$$\tilde{g}^L(0) = \tilde{M}\tilde{g}^R(0)\tilde{M}^+, \quad (2.14)$$

where  $\tilde{g}$  is a  $2 \times 2$  matrix in the directional (i.e.,  $+$   $-$ ) space with elements  $\hat{g}_{\alpha\beta}$ , each of which is a  $2 \times 2$  matrix in the particle-hole space.  $\tilde{M}$  is also a  $2 \times 2$  matrix in the

directional space, of the form:

$$\tilde{M} = \begin{pmatrix} \frac{1}{c_d} & \frac{c_r^*}{c_d^*} \\ \frac{c_r}{c_d} & \frac{1}{c_d^*} \end{pmatrix}, \quad (2.15)$$

where  $c_r$  and  $c_d$  are the reflection and transmission coefficients (*i.e.*, probability amplitudes), respectively. The boundary conditions at the two ends  $x = -L_L$  and  $x = L_R$  are [36]

$$\begin{aligned} \hat{g}_{++}^L(-L_L) + i &= \hat{g}_{--}^L(-L_L) + i = -e^{-i\eta_L} \hat{g}_{+-}^L(-L_L), \\ \hat{g}_{++}^L(-L_L) - i &= \hat{g}_{--}^L(-L_L) - i = -e^{i\eta_L} \hat{g}_{-+}^L(-L_L), \\ \hat{g}_{++}^R(L_R) + i &= \hat{g}_{--}^R(L_R) + i = -e^{-i\eta_R} \hat{g}_{-+}^R(L_R), \\ \hat{g}_{++}^R(L_R) - i &= \hat{g}_{--}^R(L_R) - i = -e^{i\eta_R} \hat{g}_{+-}^R(L_R), \end{aligned} \quad (2.16)$$

where  $\eta_L$  and  $\eta_R$  are arbitrary phase factors.

## B. Self-consistent Order Parameter

For the d-wave superconductor described in Fig. 1,  $\Delta_L(\theta, x) = \Delta_L(x) \cos(2\theta)$  and  $\Delta_R(\theta, x) = \Delta_R(x) \sin(2\theta)$ . The pair interaction function  $V(\theta, \theta')$  in Eq. (2.9) has the same symmetry as the order parameter with respect to both  $\theta$  and  $\theta'$  [*i.e.*, on the left hand side of the grain boundary,  $V(\theta, \theta') = V_d \cos(\theta) \cos(\theta')$ , and on the right hand side of the grain boundary,  $V(\theta, \theta') = V_d \sin(\theta) \sin(\theta')$ ]. From Eq. (2.9), we have

$$\Delta(x) = \frac{2T \sum_{n=0}^{\omega_c/2\pi T} \int_{-\pi/2}^{\pi/2} d\theta' \sum_{\alpha=\pm} [\lambda(\theta'_\alpha) \hat{g}_{\alpha\alpha}(x, \theta'_\alpha, \varepsilon_n)]_{12}}{\ln\left(\frac{T}{T_{cd}}\right) + \sum_{n=0}^{\omega_c/2\pi T} \frac{1}{n+0.5}}, \quad (2.17)$$

where  $\Delta(x)$  means  $\Delta_L(x)$  for the l.h.s. ( $x < 0$ ), and  $\Delta_R(x)$  for the r.h.s. ( $x > 0$ );  $\lambda(\theta) = \cos(2\theta)$  for the l.h.s. and  $\lambda(\theta) = \sin(2\theta)$  for the r.h.s.;  $\omega_c$  is a cutoff to the summation for  $\varepsilon_n$ ; The strength of the pair interaction  $V(\theta, \theta')$  has been eliminated

after we introduce  $T_{cd}$  — the transition temperature of the  $d$ -wave superconductor — by letting  $\Delta \rightarrow 0$ . [37] We solve the differential equation (2.12) and the boundary conditions (2.14) and (2.16) together with Eq. (2.17) iteratively till the self-consistency is achieved. Before numerically solving Eq. (2.12), the exponentially growing part of the solution needs to be analytically separated and removed. The technique is explained in detail in Ref. [37]. On the r.h.s. of Eq. (2.17), the numerator and the denominator depend on the cutoff frequency  $\omega_c$ . However, when  $\omega_c$  is large, though both of them are divergent, their ratio is convergent. In our calculation, we have chosen  $\omega_c = 20\pi T_{cd}$ , and we have established that the convergence has been achieved. The accuracy of the self-consistent order parameter for every point studied is 4 significant digits. When  $L_L, L_R \rightarrow \infty$ , the self-consistent order parameter is independent of the phase factors  $\eta_L$  and  $\eta_R$ , and only depends on two parameters: temperature  $T$  and the reflectivity of the interface  $r \equiv |c_r|^2$ . [37]

The order parameter tends to the constant bulk value when it's away from the interface, therefore in our calculation, we take the range of  $x$  as from -5 to 5 with unit of the coherent length  $\xi_0 \equiv \hbar v_F / \Delta_0$ . We calculate the order parameter for 1000 points in this range. We start with a constant order parameter, *i.e.* same value for each point, to solve Eqs. (2.12), (2.14), and (2.16) to obtain the Green functions, then use Eq. (2.17) to obtain a new order parameter for each point. We then use the new order parameters to repeat the calculation. The loop of the calculation will continue until the maximum difference of the order parameter for each point between two loops is less than 0.0001, *i.e.*, the self-consistence is achieved.

Fig. 2 shows the results of the self-consistent order parameter for two temperatures,  $T = 0.025T_{cd}$  and  $0.1T_{cd}$ . For each temperature, we calculate the order parameter

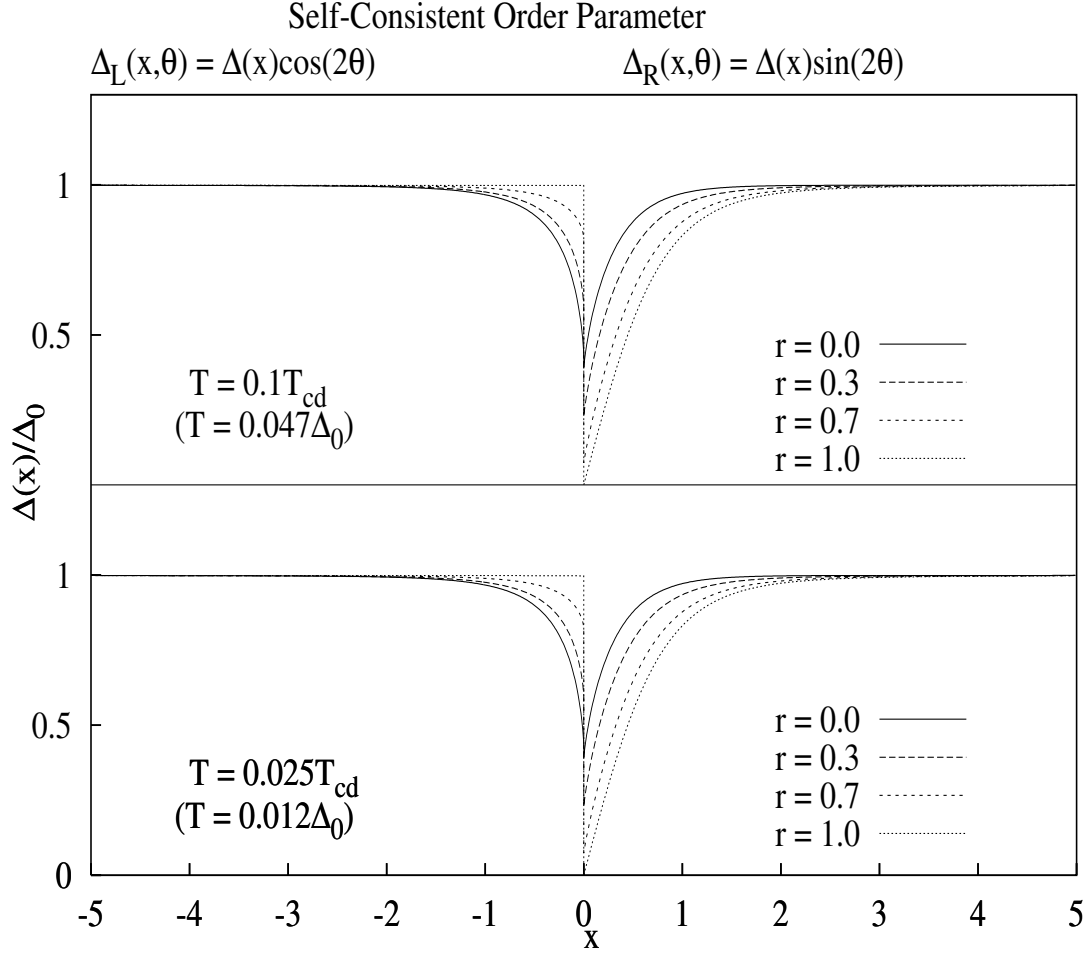


Fig. 2. Plot of the normalized self-consistent superconducting order parameter as a function of  $x$  at four values of the interface reflectivity  $r$  and two values of the temperature  $T$ : Upper panel:  $T = 0.1T_{cd}$ ; Lower panel:  $T = 0.025T_{cd}$ .

for four values of  $r$ :  $r = 0, 0.3, 0.7$  and  $1$ . The unit of  $x$  is the coherent length  $\xi_0 \equiv \hbar v_F / \Delta_0$ . When  $r = 1$ , the interface is pure reflection, so the two grains are independent of each other. In this case, the order parameter should be that of a superconductor with a specular surface on each side of the interface. The order parameter on the l.h.s. (the  $\{100\}$  side) is a constant, just like an s-wave superconductor because the incoming and outgoing quasiparticles experience the same order-parameter sign. However, for the r.h.s. (the  $\{110\}$  side), the reflected electrons see the sign change of the order parameter so there exists a pair-breaking effect. [39] Therefore, the order parameter near the interface is depressed than that in the bulk. In fact, it drops to zero at the interface. In the case of  $r < 1$ , for the l.h.s., some cooper pairs can leak into the r.h.s., which leads to some depression of the order parameter near the interface on this side. The depression increases with decreasing  $r$  because more Cooper pairs can leak into the r.h.s.. However for the r.h.s., the depression decreases with decreasing  $r$  because less probability of reflection implies less pair-breaking effect.

## CHAPTER III

### TUNNELING CHARACTERISTICS\*

#### A. N-D Tunneling

##### 1. Local Tunneling Current

We extend the tunneling Hamiltonian approach used in Ref. [9] to local tunneling characteristics. The local tunneling current between a normal metal tip and the  $d$ -wave superconductor described in Fig. 1 can be expressed by using the quasi-classical Green function:

$$I(x, V) = \frac{1}{2\pi} \int_{-\frac{\pi}{2}}^{\frac{\pi}{2}} d\theta \int_{-\infty}^{\infty} dE \mathcal{N}(E + ev) [f(E) - f(E + eV)] \times \text{Im}([\hat{g}_{++}(x, \theta_+, E) + \hat{g}_{--}(x, \theta_-, E)]_{11}, \quad (3.1)$$

where “ $\text{Im}$ ” means the imaginary part, and “11” means the element 11 of the matrices  $\hat{g}_{\alpha\alpha}$  ( $\alpha = +, -$ ). The current  $I(x, V)$  has been normalized by that of the N-N tunneling.  $V$  is the bias voltage, and  $f(x)$  is the Fermi function.  $\mathcal{N}(E)$  is the normalized density of states of the counter-electrode and  $\mathcal{N}(E) = 1$  for a normal metal tip.  $\hat{g}_{\alpha\beta}(x, \theta, E)$  is the analytical continuity of  $\hat{g}_{\alpha\beta}(x, \theta, \varepsilon_n)$ :

$$\hat{g}_{\alpha\beta}(x, \theta, E) = \hat{g}_{\alpha\beta}(x, \theta, \varepsilon_n)|_{\varepsilon_n \rightarrow -iE + \delta}, \quad (3.2)$$

with  $\delta$  being a small positive number. Inserting the Green function  $\hat{g}_{\alpha\beta}$  obtained by using the self-consistent order parameter into Eq. (3.1), we obtain the normalized tunneling conductance. We have calculated the tunneling conductance for eight dis-

---

\*Modified with permission from “Local tunneling characteristics near a grain boundary of a  $d$ -wave superconductor as probed by a normal-metal or a low- $T_c$ -superconductor STM tip” as follows: Hongwei Zhao and Chia-Ren Hu, *The Physical Review B*, 62, 1308-1318, 2000. Copyright (2000) by the American Physical Society.



tances ( $x$ 's) from the grain boundary. Four distances are on the l.h.s. of the grain boundary (*i.e.*,  $x < 0$ ), and the other four distances are on the r.h.s. (*i.e.*,  $x > 0$ ).  $\hat{g}_{\alpha\beta} = \hat{g}_{\alpha\beta}^R$  for  $x > 0$  and  $\hat{g}_{\alpha\beta} = \hat{g}_{\alpha\beta}^L$  for  $x < 0$  in Eq. (3.1). The results of the normalized conductance versus the bias voltage at temperature  $T = 0.025T_{cd}$  and four values of  $r$  ( $r = 0, 0.3, 0.7$  and  $1$ ) are shown in Fig. 3 to Fig. 6. Part (a) gives the results for the tunneling points on the l.h.s. of the grain boundary, and part (b), on the r.h.s.. The corresponding results for another temperature  $T = 0.1T_{cd}$  and  $r = 0.7$  are shown in Fig. 7. We have chosen  $\delta = 0.05T_{cd}$  in Eq. (3.2) for all of the calculations. We have also calculated the tunneling conductance by using a constant order parameter in each grain for comparison. In Figs. 3 to 6, the dash lines are the results obtained by using a constant order parameter for each side of the interface, and the solid lines are those by using the self-consistent order parameter. We can see that for a given  $r$ , the error in the results due to the use of the constant order parameters is larger when the tunneling point is closed to the interface. When the tunneling point moves away from the interface, the two results tend to be the same. This is obvious because the order parameter tends to the constant bulk value when it's away from the interface. For a fixed tunneling point on the l.h.s., this error is smaller for increasing  $r$ , and when  $r = 1$  (Fig. 6(a)), the error reduces to exactly zero, as it should be, since for  $r = 1$ , the l.h.s. has a free surface, and the self-consistent solution gives a constant order parameter. For the r.h.s., the error is larger for larger  $r$  due to the pair-breaking property of the interface.

In these figures,  $x = +0.0$  and  $x = -0.0$  mean that the tunneling occurs just to the right and left side of the interface, respectively. When  $r = 0$ , the quasi-classical Green function is continuous across the interface, so the tunneling conductance is also continuous there. Therefore, the curve for  $x = -0.0$  in Fig. 3(a) is exactly the same

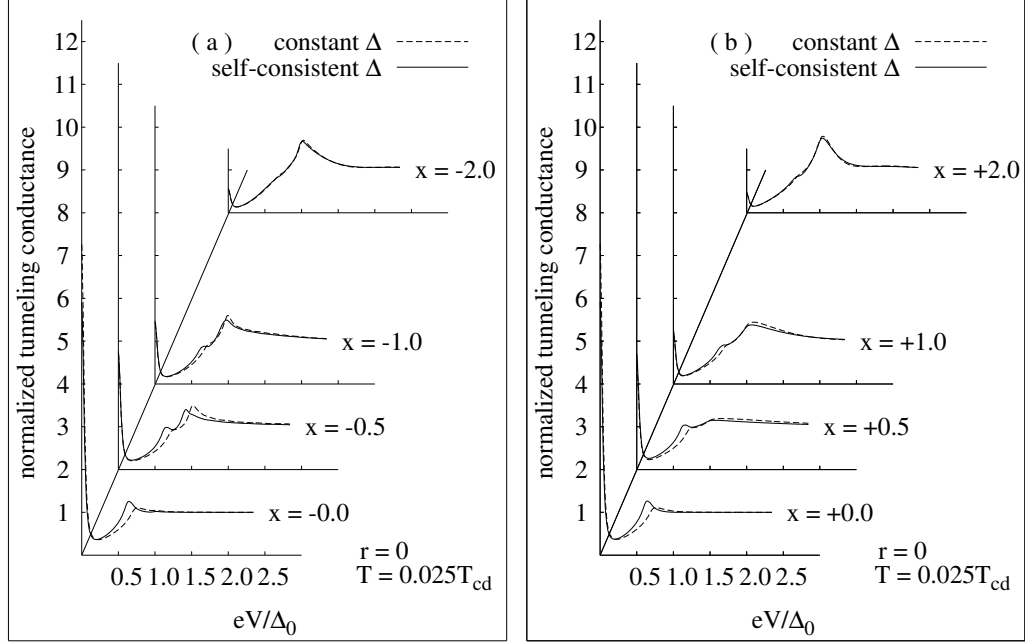


Fig. 3. Normalized local tunneling conductance  $G$  between a normal-metal STM/S tip and a  $d$ -wave superconductor with a  $\{100\}|\{110\}$  grain boundary, as a function of the applied voltage  $V$ . Part (a) is for four values of  $x$  (in units of  $\xi_0$ ) on the  $\{100\}$  side (i.e., the negative  $x$  side), and part (b) is for four values of  $x$  on the  $\{110\}$  side (i.e., the positive  $x$  side). The grain-boundary reflectivity parameter is assumed to be  $r = 0$  here, and the temperature is assumed to be  $T = 0.025T_{cd}$ . Solid lines are obtained using the self-consistent order parameter, and the dashed lines are obtained by assuming a constant order parameter on each side. A width parameter for the quasi-particle eigenstates has been taken to be  $\delta = 0.05T_{cd}$ . With 100% transmission at the grain boundary assumed here, the local conductance shows no discontinuity at  $x = 0$ .

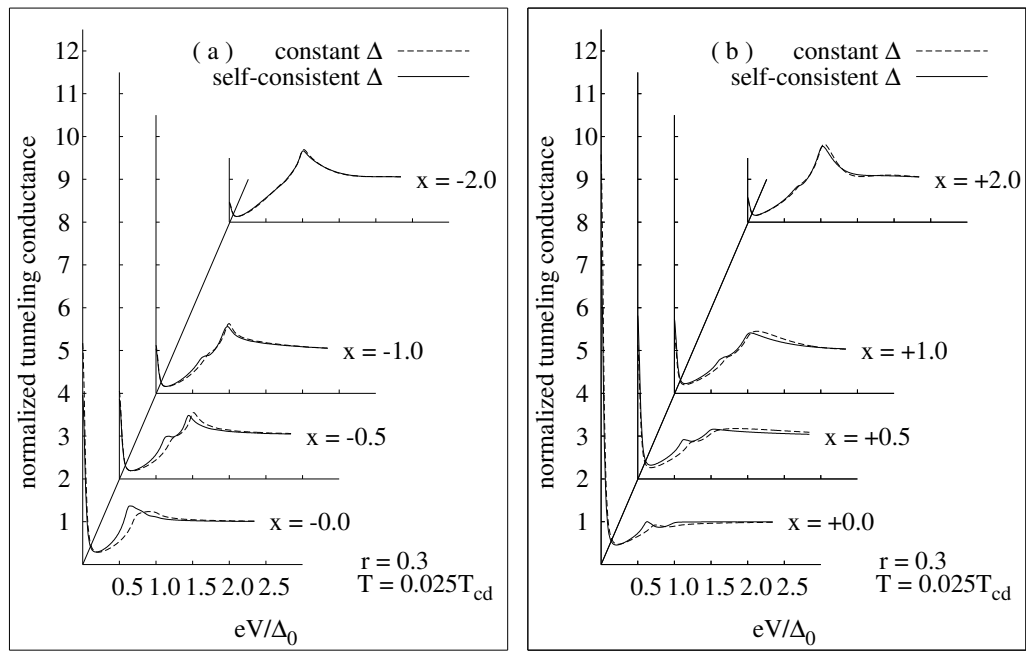


Fig. 4. Same as Fig. 3 except that  $r = 0.3$  in this figure. The local conductance is now discontinuous at  $x = 0$ . That is, the plots at  $x = \pm 0$  are now different.

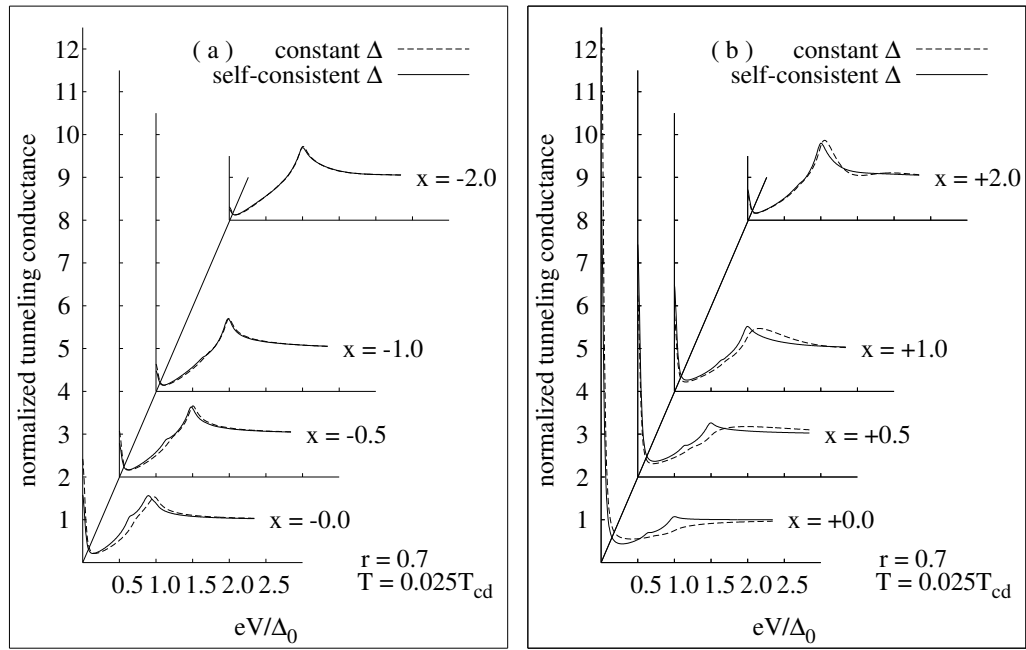


Fig. 5. Same as Fig. 4 (or 3) except that  $r = 0.7$  in this figure.

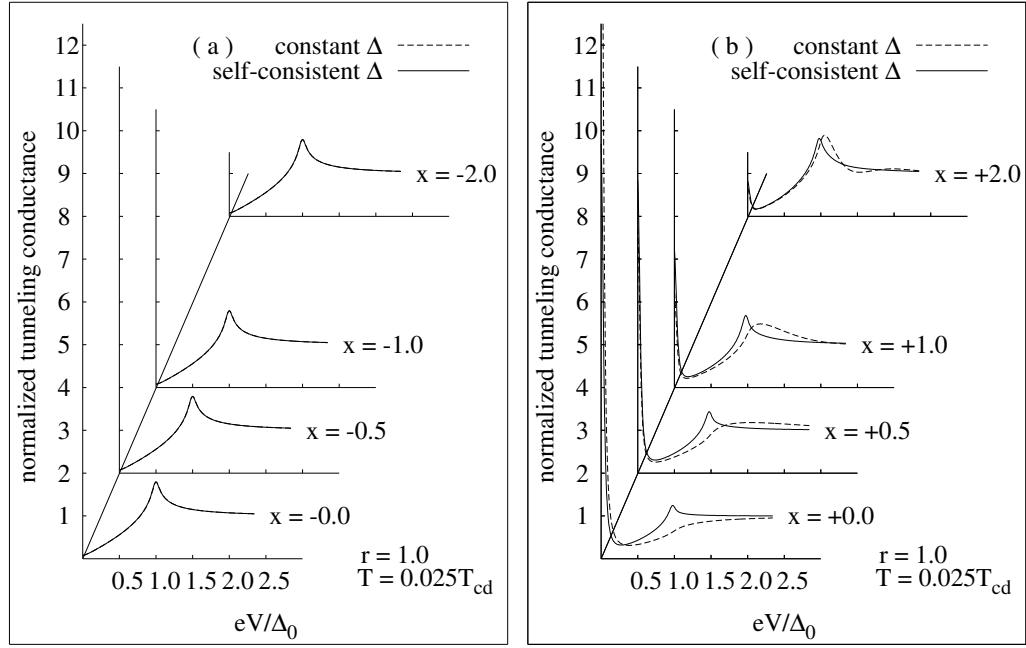


Fig. 6. Same as Fig. 4 (or 3) except that  $r = 1.0$  in this figure. This case corresponds to the sample split into a semi-infinite sample with a  $\{100\}$  surface situated at  $x < 0$ , and a semi-infinite sample with a  $\{110\}$  surface situated at  $x > 0$ . The ZBCP then shows up on the  $x > 0$  side only, near  $x = 0$ , where midgap surface states exist.

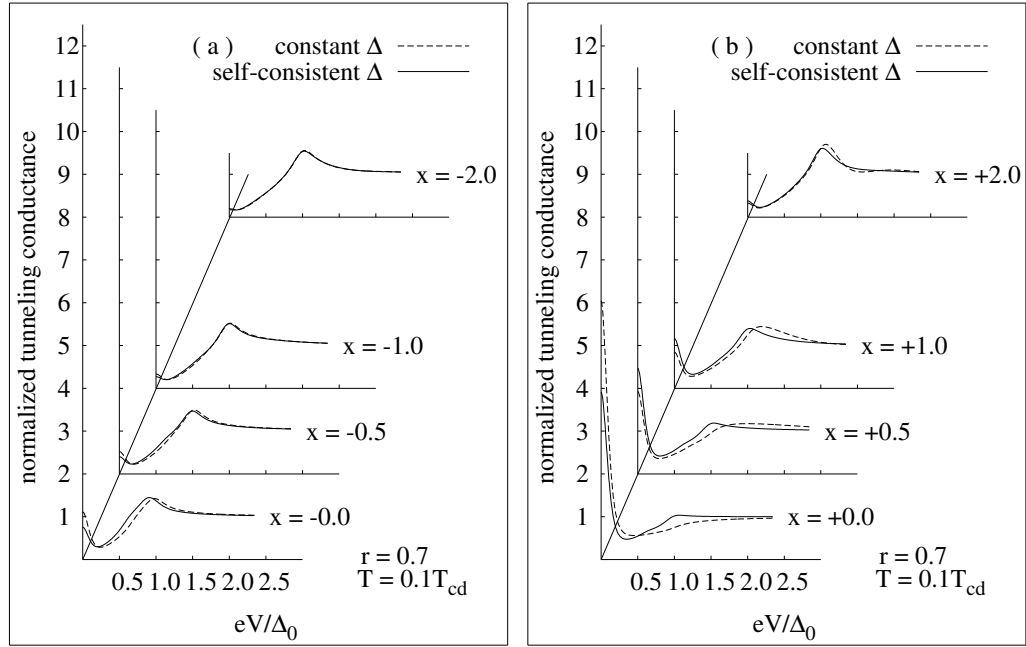


Fig. 7. Same as Fig. 5 except that the temperature  $T = 0.1T_{cd}$ . This figure is to illustrate the temperature effect.

as that for  $x = +0.0$  in Fig. 3(b). When  $r \neq 0$ , the tunneling conductance is discontinuous across the interface because of the discontinuity of the quasi-classical Green function there. Then tunneling characteristics at  $x = +0.0$  and  $x = -0.0$  are different, as may be seen in Figs. 4(a), 4(b); in Figs. 5(a), 5(b); and in Figs. 6(a), 6(b). Therefore, the ZBCP is also discontinuous (continuous) at  $x = 0$  for  $r \neq 0$  ( $r = 0$ ). This can be seen clearly in Fig. 8. When  $r = 1$ , the  $\{100\}$  side and  $\{110\}$  side are completely disconnected with each other and each of them behaves like a simple-crystal sample with a free  $\{100\}$  and  $\{110\}$  surface, respectively. For this case, there is no ZEBS's on  $\{100\}$  side, which corresponds to that there is no ZBCP on  $\{100\}$  side in Fig. 6(a).

The ZBCP corresponds to the quasi-particles tunneling into the ZEBS's. All of these figures show that the height of the ZBCP has a maximum at the interface, and diminishes when the tunneling point moves away from the interface. Observing this behavior will clearly verify that the ZEBS's are localized around the interface. (Note that the  $r = 1$  case presented in Figs. 6(a) and 6(b) corresponds to a single-crystal sample with a free  $\{100\}$  and  $\{110\}$  surface, respectively, probed by local tunneling near the surface.) The relationship between the height of the ZBCP and the distance away from the interface for different  $r$  is shown in Fig. 8. It also shows that the l.h.s. ZBCP decreases in height, and the r.h.s. ZBCP increases in height, when  $r$  increases. The relationship between the height of the ZBCP and  $r$  reflects that between the wave function of the ZEBS's and  $r$ . In Fig. 8, the ZBCP is continuous at the interface,  $x = 0$  only for  $r = 0$  because the Green function is continuous only when  $r = 0$ . This can be seen from Fig. 9.

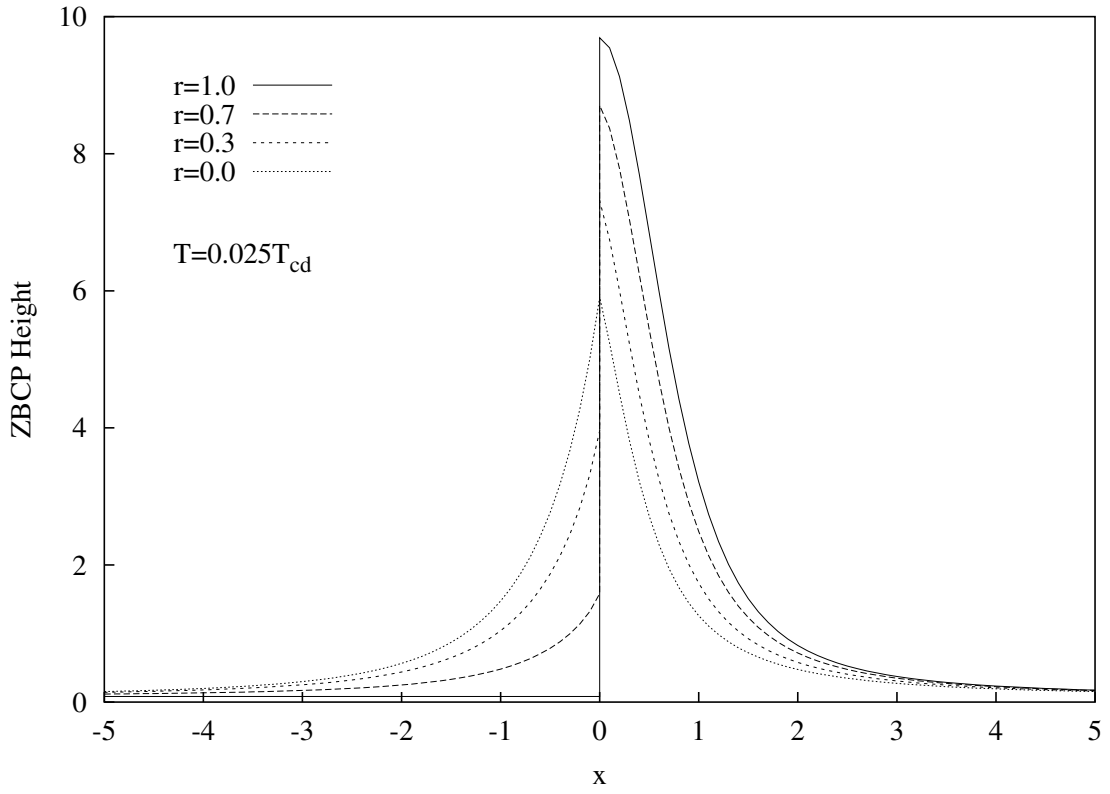


Fig. 8. The height of the ZBCP is plotted as a function of the distance  $x$  away from the interface for different values of  $r$ .  $T = 0.025T_{cd}$  is assumed.



## 2. Local Density of States

We can consider the following normalized *local* density of states[37]

$$n(x, \theta, E) = \frac{1}{4} \sum_{\alpha} \text{Im}[\text{Tr}(\hat{g}_{\alpha\alpha}(x, \theta_{\alpha}, E) \hat{\rho}_3)]. \quad (3.3)$$

For  $E = 0$ , it gives essentially the absolute-squared wave-function of the ZEBS for the given  $\theta$  because practically all of the contribution to  $n(x, \theta, E = 0)$  is from the wave function of the ZEBS for this  $\theta$  when  $\delta$  in Eq. (3.2) is very small. (But notice that it has its rapidly-oscillating component removed already.)  $n(x, \theta, E)$  in Eq. (3.3) has been normalized by the corresponding density of states of a normal metal. Fig. 9 gives a plot of this  $n(x, \theta, E = 0)$  versus  $x$  for  $r = 0, 0.3, 0.7$  and  $1$ , and in these figures we have chosen  $\theta = (3/16)\pi$ . In Fig. 9, part (a) gives the results obtained by using the self-consistent order parameter and part (b) gives those obtained by using a constant order parameter on each side of the grain boundary. It shows that  $n(x < 0, \theta, E = 0)$  decreases, and  $n(x > 0, \theta, E = 0)$  increases with increasing  $r$ , which corresponds to the l.h.s. ZBCP's height decreasing, and the r.h.s. ZBCP's height increasing, with increasing  $r$ , as shown in Fig. 8. [Actually, the  $n(x > 0, \theta, E = 0)$  calculated using the self-consistent order parameter is found to decrease when  $r$  is increased, for some angles closed to  $\pi$  and with  $x$  near the interface, as shown in Fig. 10 for  $\theta = (3/8)\pi$ . However, the ZBCP corresponds to a summation of all  $\theta$ , and the contribution from this special angular range is small in comparison with that from the remaining angular range, so the relationship between the ZBCP height and  $r$  does not show this complication.] When  $r = 1$ , only the  $\{110\}$  side (*i.e.*, the r.h.s.), can have the ZEBS's. So, all of the wave functions of the ZEBS's are located on the r.h.s., which corresponds to that the ZBCP is located on the r.h.s. in Fig. 6 and 8. From Fig. 9, we can also see that the quasi-classical Green function is continuous across

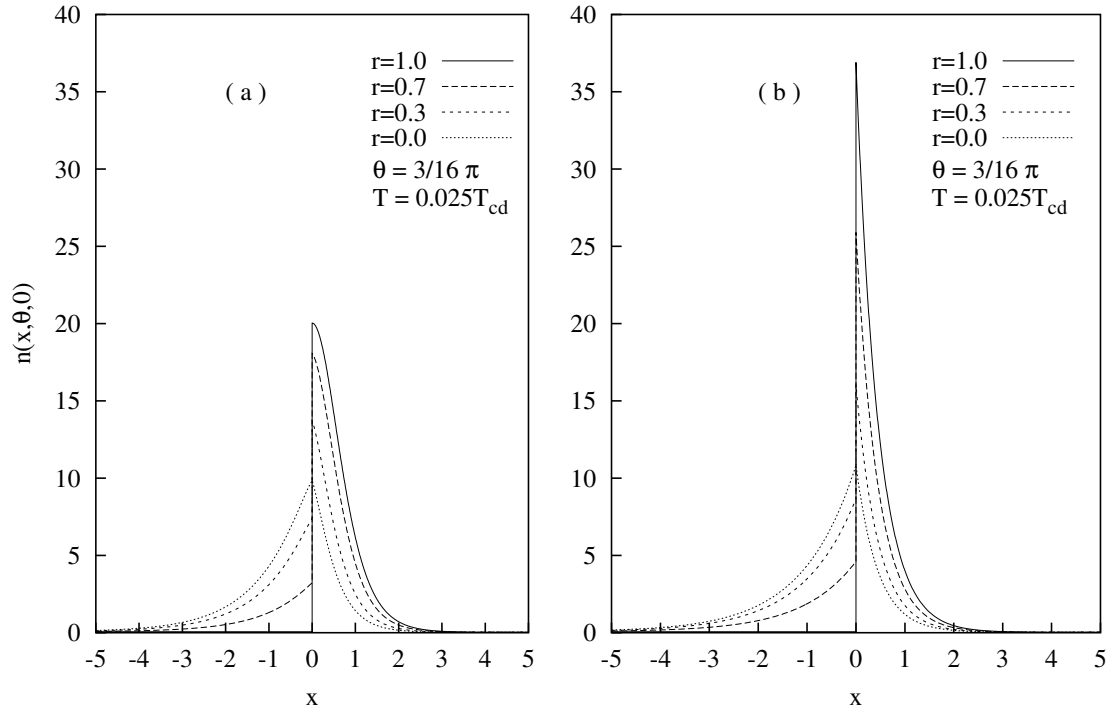


Fig. 9. Plot of  $n(x, \theta, E)$  at  $E = 0$  as a function of  $x$  for four values of  $r$  at  $\theta = (3/16)\pi$ .

Part (a) is obtained using the self-consistent order parameter, and part (b) is obtained by assuming a constant order parameter in each grain.

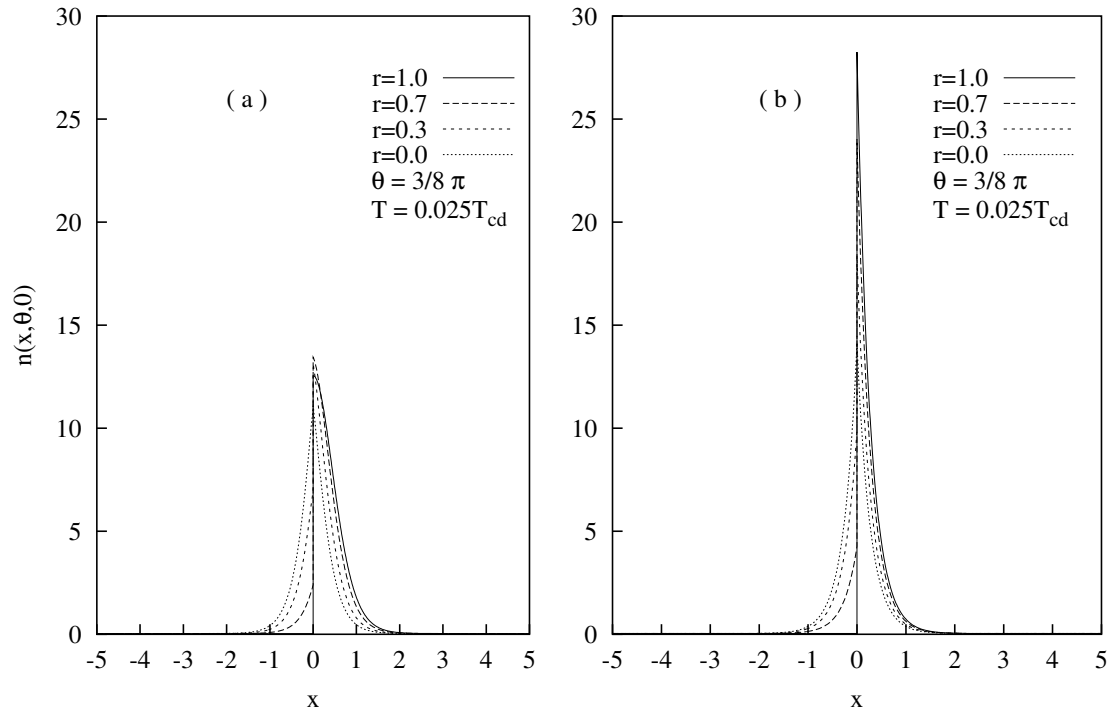


Fig. 10. Same as Fig. 9 except that  $\theta = (3/8)\pi$ .

the interface when  $r = 0$  but discontinuous when  $r \neq 0$ .

### 3. Discussions of Results

In Ref. [10], we shall discuss the conditions for the existence of the ZEBS's for a d-wave superconductor with a grain boundary. Even though in that work we considered only a constant order parameter for each side of the grain boundary, the conditions obtained there are also valid for the self-consistent order parameter because of the topological nature of the ZEBS's. [5, 7, 8, 9] In that work we have shown that for a d-wave superconductor with a  $\{100\}|\{110\}$  grain boundary, there are no "ZEBS's" with their energies shifted to non-zero energies in the WKB approximation. [10] All of the ZEBS's will remain at zero energy when  $r$  changes to any value between 0 and 1. So the apparent sub-gap peak at  $E \sim 1/\sqrt{2}$  in Figs. 3-7 is not due to any finite-energy bound states. In fact, it is from the interference between the effects of the order parameters on the two sides of the grain boundary: As long as  $r \neq 1$ , every quasi-particle can see two order parameters from the two sides of the interface. The sub-gap peak for constant order parameter is located at  $1/\sqrt{2}$ , where the quasi-particle experiences equal pair potential in both sides. The self-consistent order parameter shifts its energy away from  $1/\sqrt{2}$  only slightly. When  $r = 1$ , there is no interference between the two sides because they are completely separated. Therefore, this kind of sub-gap peak does not appear in Fig. 6. Of course, when the orientation angles of the two sides are not as chosen here, it is possible to have some "ZEBS's" shifted to non-zero energies. [10] Then we expect that the "ZBCP" will show more complex behavior, and it will be different for different  $r$ . But it may be very difficult to observe this behavior due to the faceting problem which plagues actually grain boundaries, especially when the orientations of the grains are neither  $\{100\}$  nor  $\{110\}$ .

The ZBCP corresponds to the quasi-particles tunneling into the ZEBS's. All of these figures show that the height of the ZBCP has a We have also calculated the normalized tunneling conductance at  $T = 0.1T_{cd}$  which is shown in Fig. 7. The behavior of the tunneling characteristics under the change of  $r$  is qualitatively the same as that at  $T = 0.025T_{cd}$ , so we only show the results for  $r = 0.7$  at this temperature. Comparing with  $T = 0.025T_{cd}$  for each tunneling point at the same  $r$ , the height of the ZBCP is seen to be reduced and the width is somewhat broadened. When the tunneling point is two coherent lengths away from the grain boundary, the ZBCP has almost disappeared. (Notice however that we have defined the coherence length to be  $\xi_0 = \hbar v_F / \Delta_0$  here, whereas in other works it is often defined to be  $\hbar v_F / \pi \Delta_0$ . In that scale this point is already more than six coherence lengths away from the interface.) Because the magnitude of the order parameter at  $T = 0.1T_{cd}$  is almost the same as that at  $T = 0.025T_{cd}$ , the depression and broadening of the ZBCP are practically all due to thermo-smearing.

## B. S-D Tunneling

In this section, we will study the case when the tip is a conventional, s-wave, low  $T_c$  superconductor. In this case we obtain a negative conductance for a narrow range of energy when the tunneling point is closed to the interface. Eq. (3.1) can be directly generalized to S-D tunneling by using

$$\mathcal{N}(E) = E / \sqrt{E^2 - \Delta_s^2}$$

for the low  $T_c$  superconductor tip.  $\Delta_s$  is the gap function (or pair potential) or order parameter of the low  $T_c$  superconductor. In the following calculation, we choose  $\Delta_s = 0.1\Delta_0$ , where  $\Delta_0$  is the maximum bulk order parameter for the d-wave super-

conductor.

The ZBCP corresponds to the quasi-particles tunneling into the ZEBS's. All of these figures show that the height of the ZBCP has a We calculate the tunneling current and conductance at  $T = 0.025T_{cd}$ . Fig. 11 shows the normalized tunneling conductance versus the bias voltage for  $r = 0.7$ . There are two interesting features. The first one is that the ZBCP splits into two peaks at  $eV = \pm E_s$ , where  $E_s$  is essentially the gap of the s-wave low  $T_c$  superconductor. The second, and also the more interesting one is that there is a range of negative conductance just outside the gap of the s-wave superconductor when the tunneling occurs near the interface. Fig. 12 shows the corresponding  $I$ - $V$  curves which exhibit current peaks.

The ZBCP corresponds to the quasi-particles tunneling into the ZEBS's. All of these figures show that the height of the ZBCP has a Both of the two features are due to the ZEBS's in the d-wave superconductor: When  $eV = \pm\Delta_s$ , the quasiparticles with the highest density of states in the s-wave superconductor side can tunnel into the ZEBS's on the d-wave superconductor side, so the tunneling current increases dramatically, which explains the high conductance peak at  $eV = \pm\Delta_s$ . When  $|eV| > \Delta_s$ , the quasiparticles with the highest density of states in the s-side tunnel into the gap region of the d-side, which has few available states. Only the quasiparticles with the smaller density of states in the s-side can now tunnel into the ZEBS's in the d-side. Therefore, the tunneling current is lower, which corresponds to the negative conductance in Fig. 11. The above discussion is similar to that on the tunneling characteristics of the conventional S-S tunneling, [40] but here the current peak appears at  $|eV| = \Delta_s$ , rather than at  $|eV| = |\Delta_1 - \Delta_2|$ .

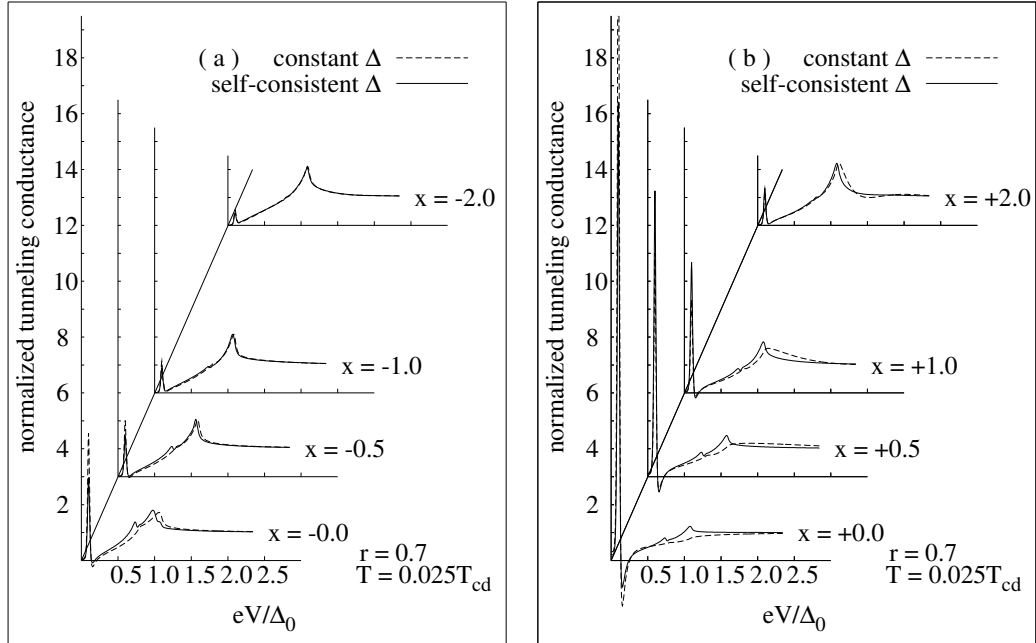


Fig. 11. Same as Fig. 5 except that the STM/S tip is now assumed to be made of a low- $T_c$   $s$ -wave superconductor with  $T_{cs} = 0.1T_{cd}$ . The temperature  $T = 0.025T_{cd}$  is  $\ll T_{cs}$  so we have approximated  $\Delta_s(T)$  by  $\Delta_s(0)$ .

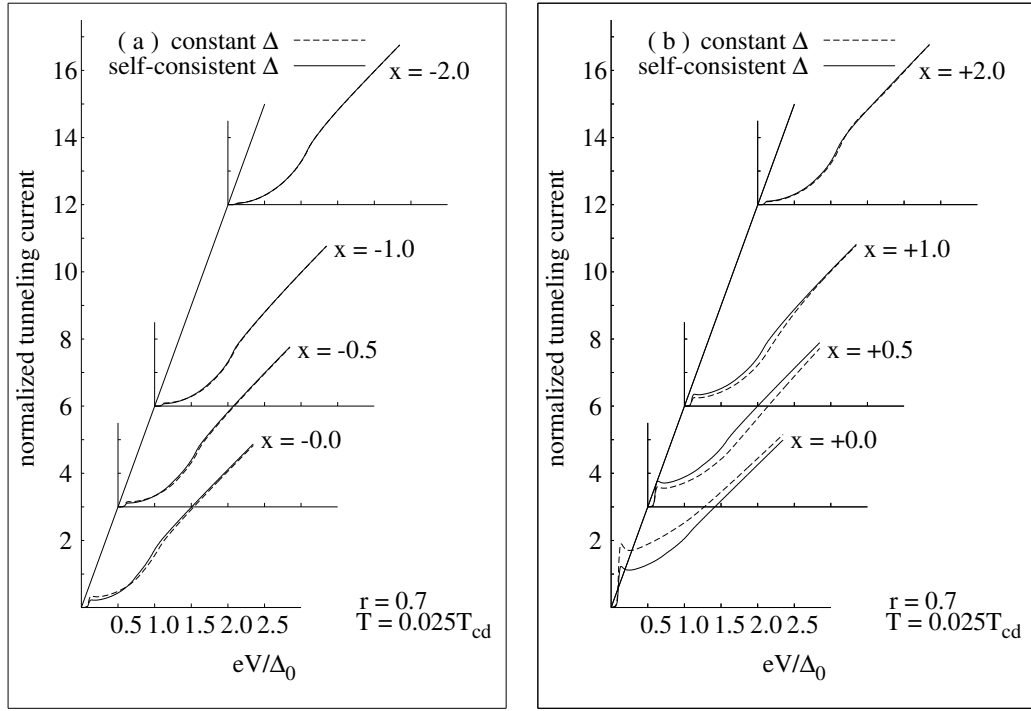


Fig. 12. The  $I(V)$  characteristics corresponding to the normalized conductance plotted in Fig. 11. The current peak in this plot gives rise to the negative conductance in Fig. 11.



The ZBCP corresponds to the quasi-particles tunneling into the ZEBS's. All of these figures show that the height of the ZBCP has a In Fig. 11, the negative conductance has larger absolute value when the tunneling point is on the r.h.s. because most part of the ZEBS wave function is localized on the r.h.s. when  $r = 0.7$ . Hurd [41] has also obtained negative conductance for  $s - d_{xy}$  tunneling. However, here we need to emphasize that because the ZEBS's are localized around a surface or interface, the negative conductance can only be observed in local tunneling near the surface or interface, and the average over even a small non-microscopic region of the sample can make the negative conductance disappear. [9] Sinha *et al.* [21] have studied the  $s$ -wave low  $T_c$  superconductor- $d$ -wave high  $T_c$  superconductor tunneling, and they saw the split ZBCP peaking at different energies at different temperatures. In order to qualitatively show this peak-energy shift at different temperatures, we have also calculated the tunneling conductance when the temperature is only slightly below  $T_{cs}$ , the critical temperature of the low  $T_c$  superconductor. The results are shown in Fig. 13. We see that the conductance at zero bias is dramatically increased and the splitting of the ZBCP is very small in comparison with the result at  $T = 0.025T_{cd}$  because the gap of low  $T_c$  superconductor is very small. (We have arbitrarily chosen the gap to be  $0.1\Delta_s$  for this calculation, which corresponds to choosing  $T = 0.97T_{cs}$ , or  $T = 0.097T_{cd}$ , since we have let  $T_{cs} = 0.1T_{cd}$ .) Sinha *et al.* [21] did not see any negative conductance. We think that it is because they studied planar junction tunneling, which measures only a spatially-averaged tunneling characteristics. We predict that negative conductance can be observed if STM/S is used to see local tunneling characteristics, if only the tunneling point is sufficiently near a surface or an interface of a  $d$ -wave superconductor where ZEBS's exist.

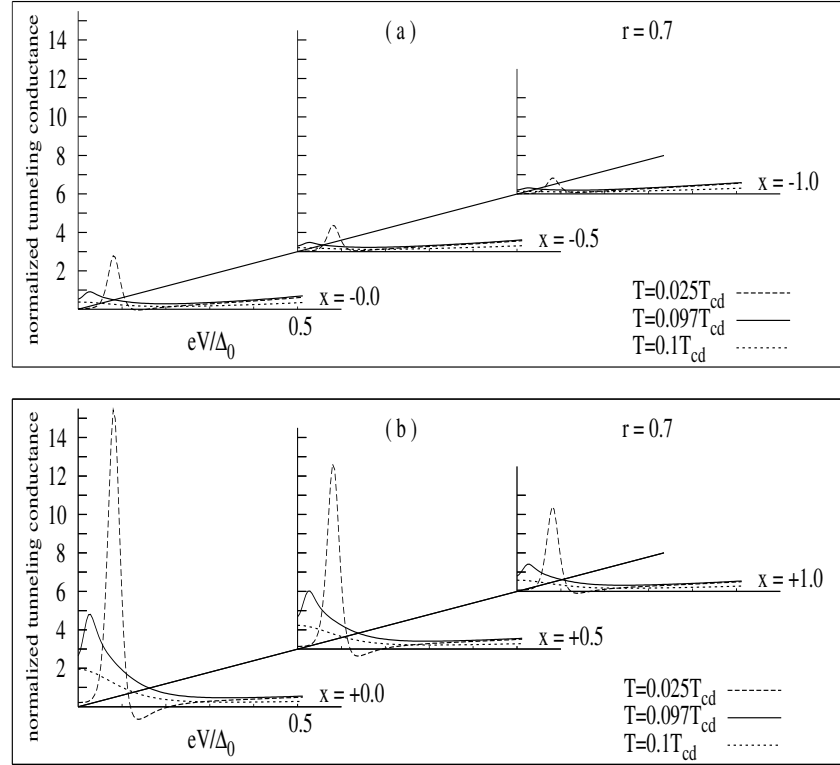


Fig. 13. Plotted is the normalized local tunneling conductance  $G$  between a low-temperature  $s$ -wave superconductor STM/S tip and a  $d$ -wave superconductor containing a  $\{100\}|\{110\}$  grain boundary as a function of the applied voltage  $V$  at six values of  $x$  (in units of  $\xi_0$ ), showing the effect of the temperature  $T$  as it is raised from much below  $T_{cs}$  ( $= 0.1T_{cd}$ ) toward  $T_{cs}$ . The gap of the low-temperature,  $s$ -wave superconductor is seen to gradually close up in the (split) zero-bias conductance peak. Part (a) is for three values of  $x$  on the  $\{100\}$  side (i.e., the  $x < 0$  side), and part (b) is for three values of  $x$  on the  $\{110\}$  side (i.e., the  $x > 0$  side). The negative conductance just outside the split ZBCP is seen to occur only at temperatures  $T \ll T_{cs}$  only.

## CHAPTER IV

## CONCLUSIONS\*

We have studied the *local* tunneling characteristics of N-D and S-D tunneling when the d-wave superconductor (D) has a  $\{100\}|\{110\}$  grain boundary, at various positions near the grain boundary. The tunneling Hamiltonian method is used to calculate the tunneling conductance, and the quasi-classical Green function method is used to obtain the self-consistency of the order parameter of the d-wave superconductor. The ZEBs are localized near the grain boundary of the d-wave superconductor. This localization can be seen in the results of our calculations: The height of the ZBCP is shown to increase when the STM/S tip moves closer to the grain boundary and decrease when it moves away from the grain boundary.

We have also calculated the tunneling characteristics assuming a constant order parameter for the d-wave superconductor in order to test how well can this approximation can be trusted. The difference between the two results varies with the position of the STM/S tip. When the tip is close to the grain boundary, the two results are more different because the self-consistent order parameter is more different from the constant value (except for the  $\{100\}$  side at  $r = 1$  where the self-consistent order parameter is and should be a constant of position.) When the tunneling tip is more than three-coherence-lengths away from the grain boundary, the two results are practically the same because the self-consistent order parameter tends to the constant bulk value

---

\*Modified with permission from “Local tunneling characteristics near a grain boundary of a *d*-wave superconductor as probed by a normal-metal or a low- $T_c$ -superconductor STM tip” as follows: Hongwei Zhao and Chia-Ren Hu, *The Physical Review B*, 62, 1308-1318, 2000. Copyright (2000) by the American Physical Society.

there (but notice that the definition for the coherence length used here does not have a factor of  $\pi$  in the denominator as some other researchers define it).

For N-D tunneling, The ZBCP has the maximum height at the interface (grain boundary) and diminishes when the tunneling point moves away from the interface. The ZBCP on the l.h.s. (*i.e.*, the  $\{100\}$  side) of the grain boundary decreases in height with the increase of the interface reflectivity  $r$ , whereas the ZBCP on the r.h.s. (*i.e.*, the  $\{110\}$  side) increases in height with increasing  $r$ . For S-D tunneling, the ZBCP splits into two peaks at  $E \simeq \pm\Delta_s$ , which reflects the gap of the s-wave low- $T_c$  superconductor, and has a range of negative conductance values just outside these peaks when the tunneling point is near the grain boundary. The s-wave gap has already been observed by non-localized tunneling, but we expect that this negative conductance just outside the gap feature can be observed only in the STM/S type of local tunneling when the tunneling point is near a surface or grain boundary of a d-wave superconductor where ZEBS's exist, assuming that temperature is sufficiently low, and there isn't a wide damaged region near the surface or interface to suppress superconductivity there. (But superconductivity can be somewhat weakened there without losing the qualitative features predicted here.)

## REFERENCES

- [1] D. A. Wollman, D. J. Van Harlingen, W. C. Lee, D. M. Ginsberg, and A. J. Leggett, Phys. Rev. Lett. **71**, 2134 (1993); C. C. Tsuei, J. R. Kirtley, C. C. Chi, L. S. Yu-Jahnes, A. Gupta, T. Shaw, J. Z. Sun and M. B. Ketchen, Phys. Rev. Lett. **73**, 593 (1994); D. A. Wollman, D. J. Van Harlingen, J. Giapintzakis, and D. M. Ginsberg, Phys. Rev. Lett. **74**, 797 (1995); J. R. Kirtley, C. C. Tsuei, J. Z. Sun, C. C. Chi, L. S. Yu-Jahnes, A. Gupta, M. Rupp, and M. B. Ketchen, Nature **373**, 225 (1995). J. R. Kirtley, C. C. Tsuei, M. Rupp, J. Z. Sun, L. S. Yu-Jahnes, A. Gupta, M. B. Ketchen, K. A. Moler, and M. Bhushan, Phys. Rev. Lett. **76**, 1336 (1996); C. C. Tsuei, J. R. Kirtley, M. Rupp, J. Z. Sun, A. Gupta, M. B. Ketchen, C. A. Wang, Z. F. Ren, J. H. Wang, and M. Bhushan, Science **271**, 329 (1996). C. C. Tsuei and J. R. Kirtley, J. Phys. Chem. Solids **59**, 2045 (1998).
- [2] D. J. Van Harlingen, Rev. Mod. Phys. **67**, 515 (1995).
- [3] J. R. Schrieffer, Solid State Comm. **92**, 129 (1994); D. G. Scalapino, Phys. Rep. **250**, 329 (1995).
- [4] C. C. Tsuei and J. R. Kirtley, Rev. Mod. Phys. **72**, 969 (2000).
- [5] C.-R. Hu, Phys. Rev. Lett. **72**, 1526 (1994).
- [6] J. Yang and C.-R. Hu, Phys. Rev. B **50**, 16766 (1994).
- [7] F. Fogelstrom, D. Rainer and J. A. Sauls, Phys. Rev. Lett. **79**, 281 (1997).
- [8] Y. Tanuma, Y. Tanaka, M. Yamashiro and S. Kashiwaya, Phys. Rev. B **57**, 7997 (1998).

- [9] C.-R. Hu, Phys. Rev. B **57**, 1266 (1998).
- [10] H. Zhao and C.-R. Hu (unpublished).
- [11] For a review, see C.-R. Hu, Int. J. Mod. Phys. B **13**, 3519 (1999).
- [12] J. Geer, X. X. Xi and G. Linker, Z. Phys. B **73**, 329 (1988).
- [13] T. Walsh, Int. J. Mod. Phys. B **6**, 125 (1992).
- [14] J. Lesueur, L. H. Greene, W. I. Feldmann, and A. Inam, Physica C **191**, 325 (1992).
- [15] Q. Chen and K.-W. Ng, Phys. Rev. B **45**, 2569 (1992).
- [16] M. Covington, R. Scheuerer, K. Bloom, and L. H. Greene, Appl. Phys. Lett. **68**, 1717 (1996).
- [17] L. Alff, H. Takashima, S. Kashiwaya, N. Terada, H. Ihara, Y. Tanaka, M. Koyanagi, and K. Kajimura, Phys. Rev. B **55**, 14757 (1997).
- [18] L. Alff, H. Takashima, S. Kashiwaya, N. Terada, T. Ito, K. Oka, Y. Tanaka, and M. Koyanagi, Physica C **282-287**, 1485 (1997).
- [19] J. W. Ekin, Y. Xu, S. Mao, T. Venkatesan, D. W. Face, M. Eddy, and S. A. Wolf, Phys. Rev. B **56**, 13746 (1997).
- [20] L. Alff, A. Beck, R. Gross, A. Marx, S. Kleefisch, T. Bauch, H. Sato, M. Naito and G. Koren, Phys. Rev. B **58**, 11197 (1998).
- [21] S. Sinha and K.-W. Ng, Phys. Rev. Lett. **80**, 1296 (1998).
- [22] L. Alff, S. Kleefisch, U. Schoop, M. Zittartz, T. Kemen, T. Bauch, A. Marx, and R. Gross, Eur. Phys. J. B **5**, 423 (1998).

- [23] M. Covington, M. Aprili, E. Paraoanu, L. H. Greene, F. Xu, J. Zhu and C. A. Mirkin, Phys. Rev. Lett. **79**, 277 (1997); M. Fogelstrm, D. Rainer, and J. A. Sauls, Phys. Rev. Lett. **79**, 281 (1997).
- [24] M. Aprili, E. Badica, and L. H. Greene, Phys. Rev. Lett. **83**, 4630 (1999).
- [25] R. Krupke and G. Deutscher, Phys. Rev. Lett. **83**, 4634 (1999).
- [26] J. Y. T. Wei, N.-C. Yeh, D. F. Garrigus and M. Strasik, Phys. Rev. Lett. **81**, 2542 (1998).
- [27] W. Wang, M. Yamazaki, K. Lee, and I. Iguchi, Phys. Rev. B **60**, 4272 (1999).
- [28] H. Aubin, L. H. Greene, S. Jian, and D. G. Hinks, Phys. Rev. Lett. **89**, 177001 (2002).
- [29] A. Kohen, G. Leibovitch, and G. Deutscher, Phys. Rev. Lett. **90**, 207005 (2003).
- [30] Z. Q. Mao, M. M. Rosario, K. D. Nelson, K. Wu, I. G. Deac, P. Schiffer, Y. Liu, T. He, K. A. Regan, and R. J. Cava, Phys. Rev. B **67**, 094502 (2003).
- [31] Y. Tanaka and S. Kashiwaya, Phys. Rev. Lett. **74**, 3451 (1995).
- [32] Y. Asano, Y. Tanaka, and S. Kashiwaya, Phys. Rev. B. **69** 214509 (2004)
- [33] S. Kashiwaya, T. Ito, K. Oka, S. Ueno, H. Takashima, M. Koyanagi, Y. Tanaka, and K. Kajimura, Phys. Rev. B **57**, 8680 (1998).
- [34] It was stated in many experimental papers that the ZBCP can only be observed in *ab*-plane tunneling, and that it can not be observed in *c*-axis tunneling. We think that such statements are misleading. Rather, we think that the only reason that the ZBCP is not observed in most *c*-axis tunneling setups is because

the total spectral weight of the ZEBS's is too small to be observable in those experimental arrangements. Thus to observe the ZBCP in  $c$ -axis tunneling all one needs to do is to increase the spectral weight of the ZEBS's, by either increasing the surface(or interface)-to-volume ratio in the sample, or, more simply, by performing *local* tunneling using STM/S in the vicinity of a surface or interface. Of course the surface can not have a thick damaged layer which is not even superconducting. But if this were the reason that the ZBCP were not observed, then the gap features should not have been observed either. The result would be the featureless, roughly-V-shaped, tunneling conductance curves reported in some (especially earlier) publications. Most recent  $c$ -axis tunneling experiments, with better prepared surfaces, were clearly not plagued by this problem, since they can all see very clear gap features.

- [35] The local density of states of N/I/D and D/I/D junctions has been studied previously by Y. Tanaka and S. Kashiwaya [Phys. Rev. B **53**, 9371 (1996)] without taking into account the self-consistency of the order parameter.
- [36] M. Ashida, S. Aoyama, J. Hara and K. Nagai, Phys. Rev. B **40**, 8673 (1989).
- [37] Y. Nagato, K. Nagai and J. Hara, J. Low Temp. Phys. **93**, 33 (1993).
- [38] Y. Ohashi, J. Phys. Soc. Jpn. **65**, 823 (1996).
- [39] C. Bruder, Phys. Rev. B **41**, 4017 (1990).
- [40] I. Giaever, in *Tunneling Phenomena in Solids*, edited by E. Burstein and S. Lundqvist (Plenum Press, New York, 1969), p. 255.
- [41] M. Hurd, Phys. Rev. B **55**, R11993 (1997).



## VITA

Hongwei Zhao was born in August, 1972, in Jilin, China. He received his B.E. degree in packaging engineering at Jilin University in June, 1993. He went to the Institute of Physics, Chinese Academy of Sciences in Beijing in September, 1993. He received his M.S. degree in physics in June, 1996. In August, 1996, he came to Texas A&M University for his graduate studies in physics. He started working in the telecommunication industry in May, 2000. At the same time, he continued his graduate studies as a part time student. He can be reached at 2320 Cimmaron Dr., Plano, TX 75025. He can also be reached by email at [hwzhao99@hotmail.com](mailto:hwzhao99@hotmail.com).